Journal of Science: Advanced Materials and Devices 4 (2019) 47–56

Contents lists available at ScienceDirect

Journal of Science: Advanced Materials and Devices

journal homepage: www.elsevier.com/locate/jsamd

Original Article

# Synthesis of silver promoted CuMnOx catalyst for ambient temperature oxidation of carbon monoxide

Subhashish Dey [a, *], Ganesh Chandra Dhal [a], Devendra Mohan [a], Ram Prasad [b]

[a] Department of Civil Engineering, IIT (BHU), Varanasi, India
[b] Department of Chemical Engineering and Technology, IIT (BHU), Varanasi, India

ARTICLE INFO

*Article history:*
Received 4 December 2018
Received in revised form
24 January 2019
Accepted 24 January 2019
Available online 1 February 2019

*Keywords:*
Hopcalite (CuMnOx) catalyst
Silver
Carbon monoxide
Deposition-precipitation
Reactive calcination

ABSTRACT

The present research shows that the addition of silver (Ag), by the deposition-precipitation method, to a mixed CuMnOx catalyst can improve the activity of carbon monoxide (CO) oxidation. The CuMnOx catalyst doped with 3 wt.% Ag shows a higher catalytic activity as compared to the 1, 2, 4 and 5 wt.% Ag doped samples. The loading of Ag could introduce new active sites into the CuMnOx catalyst and reduce its deactivation. The order of the optimal calcination strategies based on the performance of catalysts for CO oxidation is as follows: Reactive Calcination > Flowing air > Stagnant air. All the catalysts were characterized by XRD, FTIR, BET, XPS and SEM-EDX techniques. It was found that the high active surface area was one of the main factors for the high catalytic activity of the Ag-promoted CuMnOx catalyst.


## 1. Introduction

Carbon monoxide (CO) is one of the most poisonous gases present in the atmosphere. It has been targeted for a long time to remove from air. CO is a colorless, odorless, tasteless and non-irritating gas, which makes it very difficult for humans to detect [1,2]. CO is a product of the partial combustion of carbon-containing compounds. Inhaling even relatively small amounts of CO can lead to hypoxic damage and neurological injury [3]. It affects not only on human beings but also vegetation by interfering with the plant respiration and nitrogen fixation. CO is one of the main reactive trace gases in the earth's atmosphere. It influences the atmospheric chemistry as well as the climate [4]. Large amounts of CO in the world are mainly emitted from transportations, power plants, manufacturing and domestic activities [5]. It was estimated that the auto-mobile vehicular exhaust contributes the largest source of CO pollution in the developed countries [6]. As the number of vehicles on roads raised, the CO concentrations have reached an alarming level in urban areas. Therefore, with an increasing public awareness and concern for the threat to the human health and environment, many emission standards in legislation focus on regulating pollutants released by the vehicles [7].

The complete oxidation of CO at ambient temperature is very important for its applications in housing , automotive air cleaning technologies, CO detectors, gas masks for firefighters and mining industry [8–10]. A catalytic converter is an automobile emissions control device that converts poisonous gases present in the exhaust to the less poisonous gases by catalyzing a redox reaction. The performance of catalytic converter highly depends upon the types of catalyst used. In presence of catalyst, the rate of chemical reaction was increased; it acts like an agent that reduces the activation energy of reactions [11,12]. The noble metals, base metals and their metal oxides are widely used as a catalyst in the catalytic converter [13,14]. Commercial catalysts mainly used for CO oxidation present in exhaust gases are noble metals, which typically have high activity and thermal stability [15,16]. However, there are challenges for the activity at high temperature above 100 °C and susceptibility to be degraded at low temperature [17,57]. Further, noble metals are too costly to be used broadly. Therefore, more attention has been focused on developing an efficient low-cost oxidation catalyst, which are active and stable at low temperature [18,19].

Hopcalite (CuMnOx), a mixed oxide of copper (Cu) and manganese (Mn), has been efficiently employed as a catalyst for the oxidation of CO. As compared to other catalysts, the hopcalite is one of the oldest known catalysts for CO oxidation at low temperature.

* Corresponding author.
*E-mail address:* subhasdey633@gmail.com (S. Dey).
Peer review under responsibility of Vietnam National University, Hanoi.

https://doi.org/10.1016/j.jsamd.2019.01.008

It is widely used for the respiratory protection systems in various types of applications like military, mining, and space devices etc [20–22]. The structure of CuMnOx catalyst also depends on the preparation methods, Cu:Mn molar ratio, drying temperature and calcination conditions [23]. It is accepted that the oxygen species associated with copper in CuMnOx catalyst are very active and may be dominated by the low-temperature oxidation of CO [24]. The reason for the increasing catalytic activity may due to the improved specific surface area, pore volume and lattice oxygen mobility of the catalysts. The lattice oxygen associated with copper species as well as the mobility of lattice oxygen from manganese species increases the reactivity of catalyst [25]. The Cu-oxide was found to be weakly active for CO oxidation, but in conjunction with Mn-oxide in an appropriate proportion, some highly active catalyst systems could be generated [26,27]. Improvement in the activity of CuMnOx catalysts for CO oxidation has been attempted by a combination of copper, manganese with other elements like Ag, Au, Co, Ce, Ti and Zr etc. The addition of a low concentration of these elements into the CuMnOx catalyst, yet this is an approach that has confirmed valuable in other oxidation catalysts [28,29]. Silver (AgO, $Ag_2O$, $Ag_2O_3$) based catalyst is considered an attractive alternative to the other metal oxide catalysts because of its high activity and stability for low-temperature CO oxidation [30–32]. It is an excellent catalyst for various catalytic oxidation reactions, such as formaldehyde production, NOx abatement, ethylene epoxidation, partial oxidation of benzyl alcohol, selective catalytic oxidation of ammonia, oxidative coupling of methane, oxidation of styrene, selective oxidation of ethylene glycol and CO oxidation [33–35].

The activity of Ag-based catalysts is strongly depended upon their surface structure and composition. It is extremely sensitive to the preparation method, pretreatment or reaction conditions, and the size of Ag nanoparticles [36–38]. Activation of silver oxide based catalyst is often regarded as a result of the presence of various Ag–O interactions, for example, the molecular, surface and subsurface oxygen atoms, etc. The surface and subsurface oxygen atoms are reported to be the active sites for Ag based catalysts in a lot of oxidation reactions [39,40]. The oxygen pretreatment at high temperature results in the creation of subsurface oxygen atoms and activates Ag catalysts [41,42]. The role of different Ag species has also been studied, and $Ag^0$ as an active species was found to increase the catalytic activity at low temperature [43,44]. The addition of Ag into the CuMnOx catalyst leads to an increase in the surface area and also increases the number of active sites presented on the catalyst surface. Therefore, it demonstrates the better activity for CO oxidation under the ambient conditions and also increases the stability of the catalyst [45–47].

The highly dispersed Ag nanoparticles deposited on the CuMnOx catalysts were obtained by the deposition-precipitation method. The Ag promoted CuMnOx catalysts are very active for many deep oxidation reactions [48]. The Ag promoter was added with less than 5 wt.% into the CuMnOx catalyst to improve their performance for CO oxidation. The influence of doping composition on the optimization of CuMnOx catalysts was also explored. The catalytic activity of Ag promoted CuMnOx catalyst was highly influenced by the addition of Ag to the molar ratio of Cu/Mn into the CuMnOx catalyst [49].

In this work, the active species and particle size of Ag-promoted CuMnOx catalysts for low-temperature CO oxidation have been investigated. The relationship between catalytic activity and physical characteristics of the catalysts, in terms of particle size and morphology, was also discussed. The reactive calcination (RC) condition is more effective for the overall oxidation activity of CO as compared to the stagnant air (SA) and flowing air (FA) calcination conditions. The RC of the precursor was carried out by the introduction of a low concentration chemically reactive CO–Air mixture (4.5% CO) at a total flow rate of 32.5 ml $min^{-1}$ over the hot precursor in a downflow bench-scale tubular reactor [50–52]. The RC process simplified the synthetic procedure by converting two steps processes into single step process in a reactive CO-air mixture at a 300 °C. Such a single step thermal treatment of the precursor was called “RC method” by the authors.

## 2. Experimental

### 2.1. Catalyst preparation

All catalysts were prepared by the co-precipitation method. All the materials used in this work were of analytical reagent grade. A solution of manganese acetate $Mn(CH_3COO)_2.4H_2O$ was added to copper (II) nitrate ($Cu(NO_3)_2 \cdot 3H_2O$) and stirred for 1 h. The mixed solution was taken in the burette and added drop-wise to a solution of $KMnO_4$ under vigorous stirring conditions for co-precipitation purpose. The precipitate was filtered and washed several times with hot distilled water to remove all the anions [34]. Doping of (1–5 wt.%) Ag in the form of silver nitrate $Ag(NO_3)_2$ into CuMnOx catalyst was also conducted by the deposition-precipitation method. The precipitate obtained was dried at temperature 110 °C for 24 h into an oven and calcined at 300 °C for 2 h. All the precursors were calcined in three different ways: firstly, traditional method of calcination in stagnant air at 300 °C above the decomposition temperatures of the precursors for 2 h in a muffle furnace; secondly, in situ calcination in flowing air at a rate of 32.5 ml $min^{-1}$ at 300 °C for 2 h. The third-way calcination was carried out under in situ reactive calcination (RC) as described below. The catalysts synthesized as above were stored in a capped glass sample holders placed in desiccators. Reactive calcination of the precursors was carried out by the introduction of a low concentration of chemically reactive CO–Air mixture (4.5% CO) at a total flow rate of 32.5 ml $min^{-1}$ over the hot precursors. The temperature of the reactor bed was increased from room temperature to 160 °C where CO conversion has initiated. This temperature was maintained for a defined period of time and CO concentration was calculated in the exit stream of the reactor at regular intervals until 100% CO conversion was achieved. After achieving total CO conversion, the resultant catalyst was annealed for half an hour at the same temperature then the temperature was increased up to 300 °C and upheld for an hour followed by cooling to room temperature in the same environment. The nomenclature of the resulting catalysts therefore was named by the capital letter of the corresponding precursors used and the suffixes ‘$_{SA}$’, ‘$_{FA}$’ and ‘$_{RC}$’ denote the calcination conditions, e.g. in air, flowing air or by RC, respectively, as presented in Table 1.

### 2.2. Characterization

The X-ray diffraction (XRD) measurement of the catalyst was carried out by using Rigaku D/MAX-2400 diffractometer with Cu-Kα radiation at 40 mA and 40 kV. The mean crystallite size (d) of the

**Table 1**
Calcination strategy and nomenclature of the catalysts.

| Catalyst Name | Calcination Strategy | Nomenclature |
|---|---|---|
| CuMnOx doped (3 wt.% $Ag_2O$) | Stagnant air calcination | $CuMnAg_{SA3}$ |
| CuMnOx doped (3 wt.% $Ag_2O$) | Flowing air calcination | $CuMnAg_{FA3}$ |
| CuMnOx | Reactive calcination | $CuMn_{RC}$ |
| CuMnOx doped (1 wt.% $Ag_2O$) | | $CuMnAg_{RC1}$ |
| CuMnOx doped (2 wt.% $Ag_2O$) | | $CuMnAg_{RC2}$ |
| CuMnOx doped (3 wt.% $Ag_2O$) | | $CuMnAg_{RC3}$ |
| CuMnOx doped (4 wt.% $Ag_2O$) | | $CuMnAg_{RC4}$ |
| CuMnOx doped (5 wt.% $Ag_2O$) | | $CuMnAg_{RC5}$ |

catalyst was calculated from the line broadening of the most intense reflection using the Debye-Scherrer equation. It provides the information about the phase, crystal orientation, structure, lattice parameters, crystallite size, strain and crystal defects etc.

$$d = 0.89\lambda/\beta\cos\theta \quad (1)$$

where d is the mean crystallite diameter, 0.89 is the Scherrer constant, l is the X-ray wavelength (1.54056 Å), and b is the effective line width of the observed X-ray reflection, calculated by the expression $\beta^2 = B^2 - b^2$ (where B is the full width at half maximum (FWHM), b is the instrumental broadening) determined through the FWHM of the X-ray reflection at 2θ of crystalline $SiO_2$. The Fourier transform infrared spectroscopy (FTIR) analysis was done by the Shimadzu 8400 FTIR spectrometer in the range of 400–4000 $cm^{-1}$ μ. The scanning electron microscope (SEM) image of as-fabricated catalyst was recorded on Zeiss EVO 18 (SEM) instrument. The accelerating voltage was used at 15 kV and magnification of the image 5000× was applied. The X-ray photoelectron spectroscopy (XPS) analysis of the catalyst was measured with Amicus spectrometer equipped with Al Kα X-ray radiation at a current of 12 mA and voltage of 15 kV to measure the binding energy used for the calibration of adventitious carbon C (1s) present in the catalyst. The C (1s) peak is often used as an internal standard for the calibration of the binding energy scale. The Brunauer Emmett Teller Analysis (BET) provides information about the specific surface area, pore volume and pore size of the catalyst. The isotherm was recorded by micromeritics ASAP 2020 analyzer and physical adsorption of $N_2$ at the temperature of liquid nitrogen (−196 °C) with a standard pressure range of 0.05–0.30 $P/P_o$.

### 2.3. Catalytic activity measurement

The conversion of CO was carried out under the following reaction conditions: 100 mg of catalyst was diluted to α-alumina with feed gas consisting of a lean mixture of (2.5 vol.% CO in air) and total flow rate was maintained at 60 mL $min^{-1}$. The air feed into the reactor was made free from moisture and $CO_2$ by passing through CaO and KOH pellet drying towers. The catalytic experiment was carried out under the steady-state conditions and the reaction temperature was increased from room temperature to 300 °C with a heating rate of 2 °C/min. The flow rate of CO and air passing through the catalyst presented in the reactor was monitored by the digital gas flow meters. The CO conversion was analyzed by the gas chromatogram to measure the activity of the resulting catalyst. Pure α–alumina spheres were used in the preheating section and the section after the catalyst bed. Eq. (2) represents the air oxidation of CO over the catalyst. The heating temperature of the catalyst presented in a reactor was controlled by a microprocessor-based temperature controller as shown in Fig. 1. The gaseous products produced after the oxidation reaction was analyzed by an online gas chromatogram (Nucon series 5765) equipped with a flame ionization detector (FID) detector, porapak q-column and a methaniser for measuring the concentration of CO and $CO_2$. FID consists of a stainless steel jet, when the carrier gas passing through the column mixed with hydrogen and burns at the tip of the jet. Hydrocarbons and other molecules which ionize in the flame were concerned to a metal collector electrode located just to the side of the flame. The resulting electron current was amplified by a special electrometer amplifier which converts very small currents to millivolts. The FID is sensitive to almost all of molecules that contain hydrocarbons.

FID is a destructive detector the effluent passing from the column mixed with hydrogen and air, and ignited. FIDs were mass sensitive rather than concentration sensitive.

$$2CO + O_2 \rightarrow 2CO_2 \quad (2)$$

where, the concentration of CO was proportional to the area of chromatogram $A_{CO}$. The overall concentration of CO in the inlet stream was proportional to the area of $CO_2$ chromatogram.

$$(X_{CO}) = [(C_{CO})_{in} - (C_{CO})_{out}] / [C_{CO}]_{in} = [(A_{CO})_{in} - (A_{CO})_{out}] / [A_{CO}]_{in} \quad (3)$$

The oxidation of CO at any instant was measured on the basis of values of the concentration of CO $(C_{CO})_{in}$ in the feed and the concentration of $CO_2$ $(C_{CO})_{out}$ in the product stream by the above Eq. (3). Where the change in the concentration of CO due to oxidation at any instant $[(C_{CO})_{in} - (C_{CO})_{out}]$ was proportional to the area of chromatogram of $CO_2$ formed at that instant $[(A_{CO})_{in} - (A_{CO})_{out}]$ and the concentration of CO in the inlet stream $(C_{CO})_{in}$ was proportional to the area of chromatogram of $CO_2$ formed $(A_{CO})_{out}$ by the oxidation of CO.

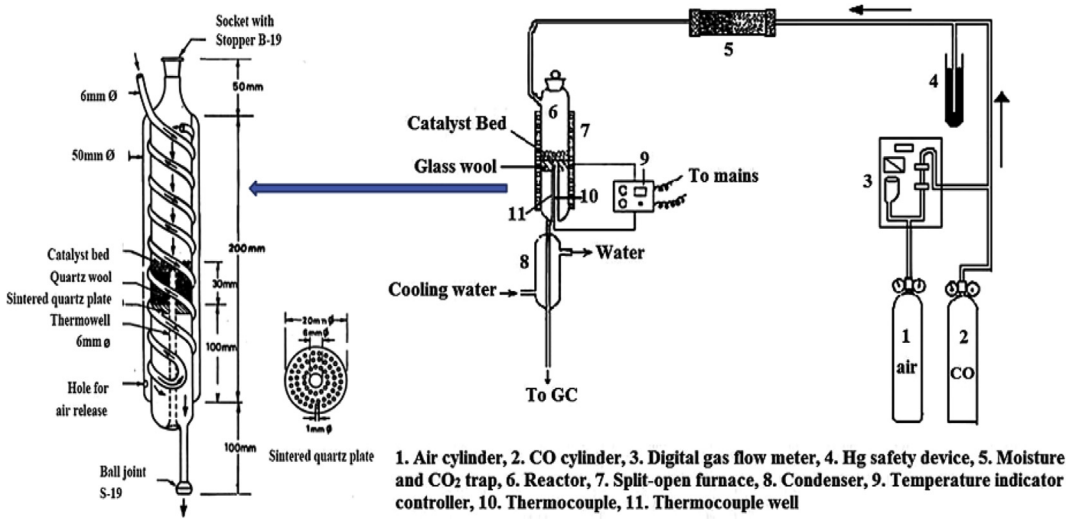


**Fig. 1.** Schematic diagram of experimental set up.

## 3. Catalyst characterization

Characterization of the catalyst samples prepared in different calcination conditions was done by the following techniques and their activity for CO oxidation was discussed below (Fig. 1).

### 3.1. Phase identification and cell dimensions

The phase identification and cell dimensions of the CuMnOx catalysts prepared in reactive calcination conditions were done by the X-ray powder diffraction (XRD) technique. It was carried out to identify the crystallite size and coordinate dimensions present in the catalysts. XRD patterns of the (3 wt.%) Ag promoted CuMnOx catalysts produced by various calcination conditions was shown in Fig. 2. In the $CuMn_{RC}$ catalyst, the diffraction peak at 2θ was 32.57, corresponds to its lattice plane (103), (130), (101), (113), (133), (011) (101) and (100) of cubic centered $Cu_1Mn_8O_4$ (PDF-75-1010 JCPDS file) and crystallite size of the catalyst was about 3.14 nm. In the $CuMnAg_{SA3}$ catalyst, the diffraction peak at 2θ was 32.60, corresponds to its lattice plane (131), (101), (113), (133), (011), (101) and (100) of face centered cubic $CuMn_8(Ag_2O)$ phase (PDF-82-1023 JCPDS file) and crystallite size of the catalyst was approximately 3.40 nm.

In the $CuMnAg_{FA3}$ catalyst, diffraction peak at 2θ was 32.54, corresponds to its lattice plane (131), (101), (113), (133), (011), (101) and (001) of face-centered cubic $CuMn_8(Ag_2O)$ phase (PDF-82-1023 JCPDS file) and crystallite size of catalyst was 2.85 nm. In the $CuMnAg_{RC3}$ catalyst, the diffraction peak at 2θ was 32.48, corresponds to its lattice plane (131), (101), (113), (133), (011), (101) and (001) of face-centered cubic $CuMn_8(Ag_2O)$ phase (PDF-82-1023 JCPDS file) and crystallite size of the catalyst was 2.4 nm. Refinement of the XRD pattern of $CuMnAg_{RC3}$ catalyst has showed that there is no impurity presented in the catalyst. The broader peak in $CuMnAg_{RC3}$ implies the relatively amorphous nature of the catalyst and their structure, phase and crystallite size was also discussed in Table 2. XRD analysis confirms that the crystallite size of $CuMnAg_{RC3}$ is smaller than other catalysts so that it may give better result for CO oxidation (Table 3).

The crystallite size of particles presented in the catalysts obtained by RC conditions was as follows: $CuMnAg_{SA3}$ > $CuMn_{RC}$ > $CuMnAg_{FA3}$ > $CuMnAg_{RC3}$. The peak widths obtained by the Scherrer equation shows that the mean crystallite size of the $CuMnAg_{RC3}$catalyst was 2.40 nm, and diffraction peaks were associated with these values could be relatively large. The particles presented in $CuMnAg_{RC3}$ catalyst were most crystalline, and producing narrow width and high-intensity diffraction linesas compared to other catalysts.

**Table 2**
XRD analysis of $CuMn_{RC}$ and CuMnAg catalysts.

| Catalyst | Structure | Phase | Crystallite size |
|---|---|---|---|
| $CuMn_{RC}$ | Cubic-centered | $Cu_1Mn_8O_4$ | 3.14 nm |
| $CuMnAg_{SA3}$ | Face-centered cubic | $CuMn_8(Ag_2O)$ | 3.40 nm |
| $CuMnAg_{FA3}$ | Face-centered cubic | $CuMn_8(Ag_2O)$ | 2.85 nm |
| $CuMnAg_{RC3}$ | Face-centered cubic | $CuMn_8(Ag_2O)$ | 2.40 nm |

**Table 3**
Particle size of catalysts.

| Catalyst | Particle size (μm) |
|---|---|
| $CuMn_{RC}$ | 3.415 |
| $CuMnAg_{SA3}$ | 4.137 |
| $CuMnAg_{FA3}$ | 2.012 |
| $CuMnAg_{RC3}$ | 1.102 |

### 3.2. Identification of the materials presented in a catalyst

The identification of the metal-oxygen bonds presented in the catalyst was done by the Fourier transforms infrared spectroscopy (FTIR) analysis. The different peaks shows various types of chemical groups presented in the catalysts. The FTIR transmission spectrum of $CuMn_{RC}$ and $CuMnAg_{RC3}$ catalysts synthesized by reactive calcination condition was showed in Fig. 3. In $CuMn_{RC}$ catalyst at the transmittance conditions, there were totally five peaks obtained. The IR band (3480 $cm^{-1}$ and 540 $cm^{-1}$) shows $Cu_2O$ group, (1640 $cm^{-1}$) $MnO_2$ group, (2340 $cm^{-1}$) C=O group and (1180 $cm^{-1}$) C-C vibration bond. In $CuMnAg_{RC3}$ catalyst at the transmittance conditions, there were totally five peaks obtained, the IR band (3480 $cm^{-1}$ and 540 $cm^{-1}$) show $Cu_2O$ group, (1640 $cm^{-1}$) $MnO_2$

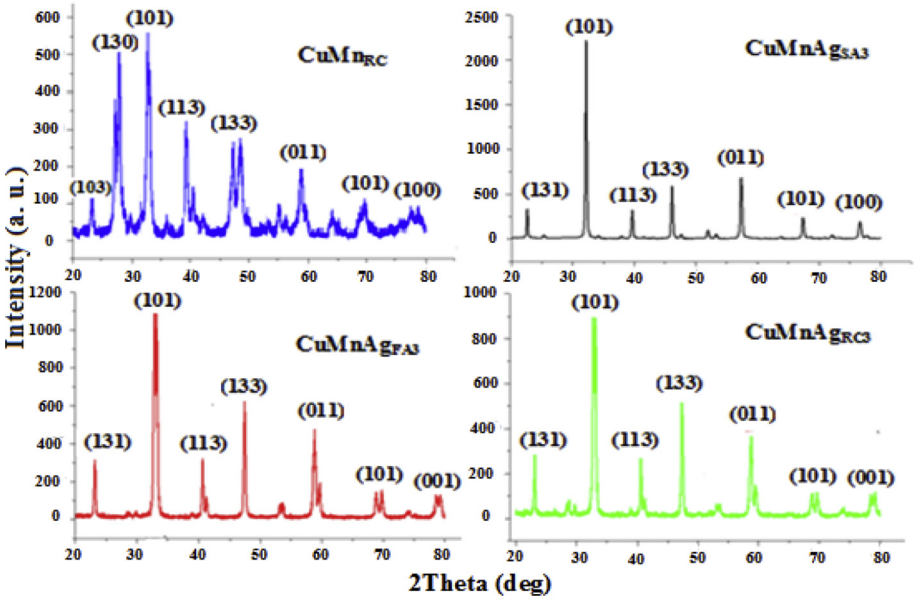


**Fig. 2.** XRD patterns of the catalysts.

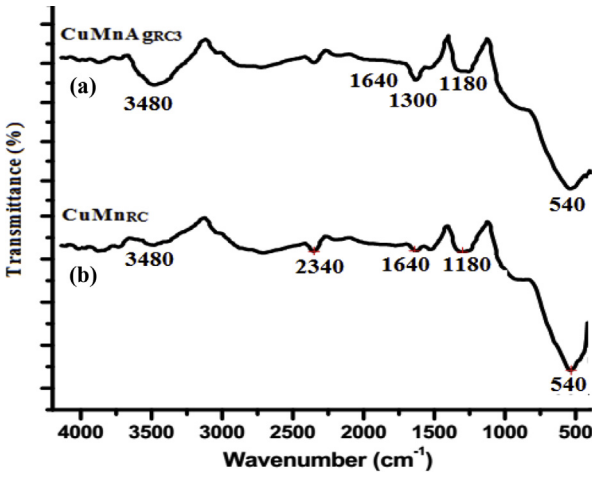


**Fig. 3.** FTIR spectra of the catalysts (a) $CuMnAg_{RC3}$ and (b) $CuMn_{RC}$.

group, (1300 $cm^{-1}$) show Ag nano-particles and (1180 $cm^{-1}$) C-C vibration bond (Fig. 4).

The $Cu_2O$ group, $MnO_2$ group and C-C bond are present in all catalysts samples. The spectra of impurities decrease in the following order: $CuMn_{RC}$ > $CuMnAg_{RC3}$. The best result obtain from FTIR analysis of $CuMnAg_{RC3}$ catalyst was free from impurity; therefore, the performance of catalyst has been increased [53,54]. All the catalysts are originates from the stretching vibrations of the metal-oxygen bonds. The adsorption strength and adsorption capacity of CO on the catalyst surfaces depend upon the homogenous dispersion of Cu and Mn components. When the adsorption capacity is moderate, thereby good catalytic activity exhibited [55,56].

### 3.3. Morphology analysis

The Scanning Electron Micrographs (SEM) instrument was used for the microstructure analysis of the optimized CuMnOx ($Cu_1Mn_8$) catalyst prepared in different calcination conditions. The promotion of Ag into the CuMnOx catalyst highly affects the morphology, particle size and porosity of the resulting catalysts. The size of particles presented in $CuMnAg_{SA3}$ catalysts produced by stagnant air calcination was comparatively large, agglomerated and homogeneous nature as compared to catalysts produced in flowing air as well as in reactive calcination conditions. The particle size in increasing order of the catalysts was as follows: $CuMnAg_{RC3}$ < $CuMnAg_{FA3}$ < $CuMn_{RC}$ < $CuMnAg_{SA3}$. The particle size of $CuMnAg_{RC3}$ catalyst was 1.102 μm, which was smallest as compared to other catalysts. Due to the smaller particle size of $CuMnAg_{RC3}$ catalyst, more and more CO chemisorbed on their surfaces. Therefore, the performance of catalyst has been increased.

The surface rebuilding behavior of different particles presented in a catalyst surfaces is observed during the period of prolonged exposure of CO gas. The $CuMn_{RC}$ and $CuMnAg_{RC3}$ catalysts produced under reactive calcination conditions show the huge differences in the microstructure and morphology on their surfaces. The doping of CuMnOx catalyst by a little amount of Ag was more efficient in improving the catalytic activity for CO oxidation. It was evenly dispersed in the micrometer range on the CuMnOx catalyst surface regardless of the reaction temperature.

### 3.4. Elemental analysis

In the CuMnOx catalysts, the percentages of different elements were analyzed by the Scanning Electron Microscopy (SEM) coupled with Energy Dispersive X-Ray analysis (SEM-EDX) techniques.

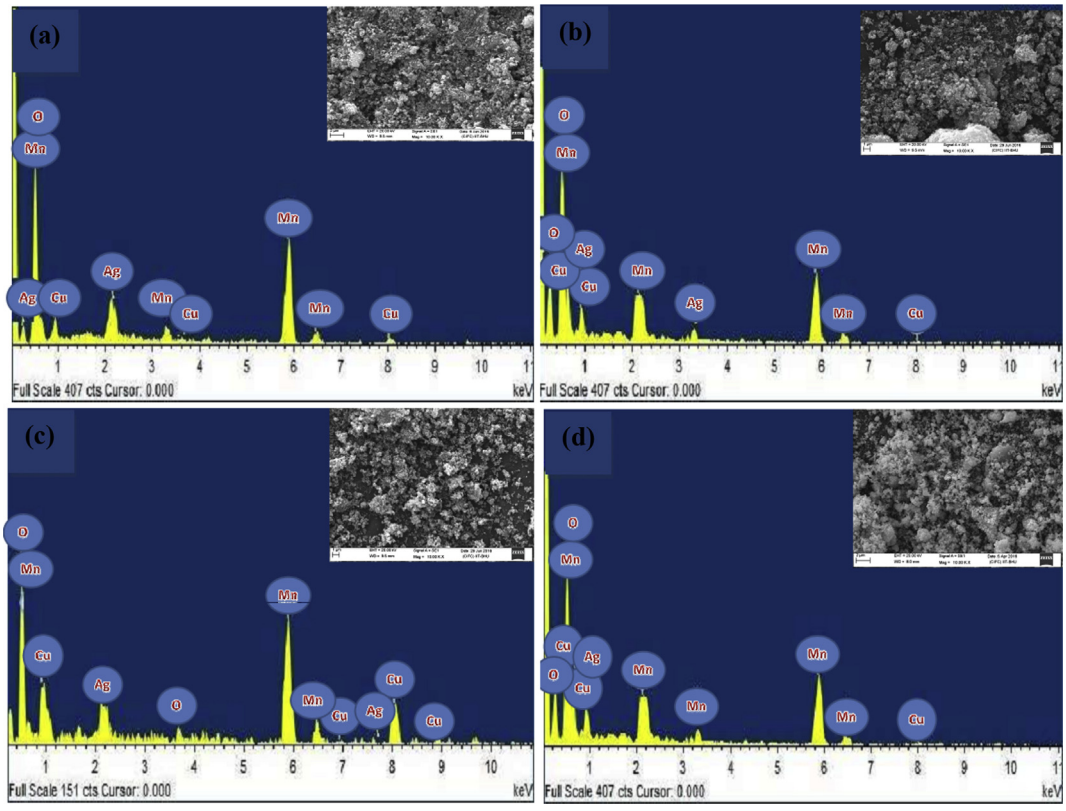


**Fig. 4.** SEM-EDX images of A) $CuMnAg_{SA3}$, B) $CuMnAg_{FA3}$ C) $CuMnAg_{RC3}$ and C) $CuMn_{RC}$ catalyst.

**Table 4**
The atomic and weight percentage (%) of the catalysts by EDX analysis.

| Catalyst | Atomic percentage (%) | | | | Weight percentage (%) | | | |
|---|---|---|---|---|---|---|---|---|
| | Cu | Mn | Ag | O | Cu | Mn | Ag | O |
| $CuMn_{RC}$ | 13.15 | 81.29 | – | 5.56 | 17.87 | 80.53 | – | 1.60 |
| $CuMnAg_{RC3}$ | 9.65 | 79.19 | 2.72 | 8.44 | 9.57 | 79.28 | 2.85 | 8.30 |
| $CuMnAg_{FA3}$ | 14.75 | 71.98 | 2.45 | 10.82 | 12.47 | 75.56 | 2.61 | 9.36 |
| $CuMnAg_{SA3}$ | 18.63 | 66.46 | 2.21 | 12.70 | 16.89 | 70.23 | 2.19 | 10.69 |

The elemental concentration distribution of the catalyst granules was determined by using Isis 300 software. The result of SEM-EDX analysis has showed that all catalyst samples were pure due to the presence of their relevant elemental peaks only. This negligible dispersion indicates that the cell unit of silver (Ag) was hardly affected by the presence of a dopant element, therefore it was confirmed that the dispersion among Ag crystallites did not create a true solid solution. The doping metals associated with CuMnOx catalyst promoted the oxygen storage, released and improved the oxygen mobility. The occurrence of oxygen deficiency in the $CuMnAg_{RC3}$ catalyst was lowest, which makes the high density of active sites. Therefore, it has to shows the best catalytic activity for CO oxidation. A calcination strategy of the CuMnAg catalysts was highly influenced by the elemental distribution of different elements presented on the catalyst surfaces. From Table 4, the relative atomic percentage of Cu, Mn, Ag and O species presented in the surface layer of CuMnAg catalysts was seen. The atomic and weight percentage of Mn was also higher than Cu, Ag and O in all the catalyst samples. The atomic percentage of Ag in the $CuMnAg_{RC3}$, $CuMnAg_{FA3}$ and $CuMnAg_{SA3}$ catalyst was 2.72, 2.45, and 2.21%, respectively, and the weight percentage of Ag in the $CuMnAg_{RC3}$, $CuMnAg_{FA3}$ and $CuMnAg_{SA3}$ catalyst was 2.85, 2.61 and 2.19%, subsequently.

However, the atomic composition of Cu, Mn and Ag in the $CuMnAg_{RC3}$ catalyst was much closer to the stoichiometric ratio of preparation rather than the $CuMnAg_{FA3}$ and $CuMnAg_{SA3}$ catalyst. The atomic percentage of oxygen presented in the CuMnAg catalyst at different calcination conditions was decreased in the following order: $CuMnAg_{RC3} > CuMnAg_{FA3} > CuMnAg_{SA3}$.

The oxygen content of the $CuMnAg_{RC3}$ catalyst was smallest as compared to the $CuMnAg_{FA3}$ and $CuMnAg_{SA3}$ catalysts. This indicates the presence of oxygen deficiency in the $CuMnAg_{RC3}$ catalyst, which may results in the high density of active sites. It was finally confirmed that the presence of pure oxides phases on the catalyst surfaces was also a good harmony with the XRD and FTIR results also.

### 3.5. Identification and quantification of elements

The XPS analysis was mainly used to understand the physical and chemical changes of catalysts by exposure of gaseous molecules under different thermal conditions. Although it can be proposed that the high binding energy was preferably for CO oxidation. The XPS spectra of Cu(2p) region is showed in Fig. 5. By performing peak fitting deconvolution of the main Cu(2p) in all catalyst samples, it was found that $Cu(NO_3)_2.3H_2O$ usually decomposed into Cu(II) oxide form after reactive calcination conditions. The prominent peak of Cu(2p) in $CuMn_{RC}$ and $CuMnAg_{RC3}$ was deconvoluted into three peaks centered. The binding energy peak of Cu(2p) in $CuMn_{RC}$ catalyst was 942.76, 937.15 and 932.15eV and $CuMnAg_{RC3}$ catalyst was 943.15, 937.24 and 932.40eV, respectively. The highest binding energy peak of Cu(2p) in $CuMn_{RC}$ and $CuMnAg_{RC3}$ catalyst was 942.76 and 943.15 eV, respectively. It was clear from Table 5 and Fig. 5 that the binding energy peak of Cu(2p) in $CuMnAg_{RC3}$ was highest in comparison with $CuMn_{RC}$ catalyst (Table 6).

XPS spectra of Mn (2p) region was represented in Fig. 5. It was observed that $Mn(CH_3COO)_2.4H_2O$ usually decomposed into $MnO_2$ form in reactive calcination conditions. The observed binding energy of Mn (2p) in $CuMn_{RC}$ and $CuMnAg_{RC3}$ catalyst was 641.63 and 640.23eV, and 641.70eV and 640.40eV, respectively, and it will be associated with the presence of $Mn^{3+}$ and $Mn^{2+}$ in all samples. The broad $Mn^{3+}$ peak was present in $CuMn_{RC}$ which indicated that the composition of $Mn^{3+}$ was higher than $CuMnAg_{RC3}$ catalyst. The highest intensity peak of Mn (2p) in $CuMn_{RC}$ and $CuMnAg_{RC3}$ catalyst was 641.63 and 641.70 eV, respectively.

The binding energy of Mn (2p) in $CuMnAg_{RC3}$ was highest as compared to $CuMn_{RC}$ catalyst. After XPS analysis of Cu and Mn elements, it is confirmed that at least some of the $Cu^{2+}$ and $Mn^{3+}$ phase was existed near the surface of catalysts. The opportunity of having surface Mn atoms in oxidation states more than 3+ is signified by the corresponding electron binding energy values and the O/Mn atomic ratio. The binding energy value of O (1s) in $CuMn_{RC}$ and $CuMnAg_{RC3}$ catalyst was 531.64 and 530.02 eV, and 531.60 and 529.86 eV, respectively, and the presence of lattice oxygen was very small in reactive calcined $CuMnAg_{RC3}$ catalyst. The amounts of oxygen presented in $CuMnAg_{RC3}$ catalyst was least as compared to $CuMn_{RC}$ catalyst. The content order of $O_a/(O_a + O_l)$ ratio was showed as follows: $CuMnAg_{RC3} > CuMn_{RC}$.

The high amount of surface chemisorbed oxygen (most active oxygen) was preferable for increasing the catalytic activity for CO oxidation. One CO molecule adsorbed on one Ag site, therefore the bridged bond accounted highest in Ag promoted CuMnOx catalyst.

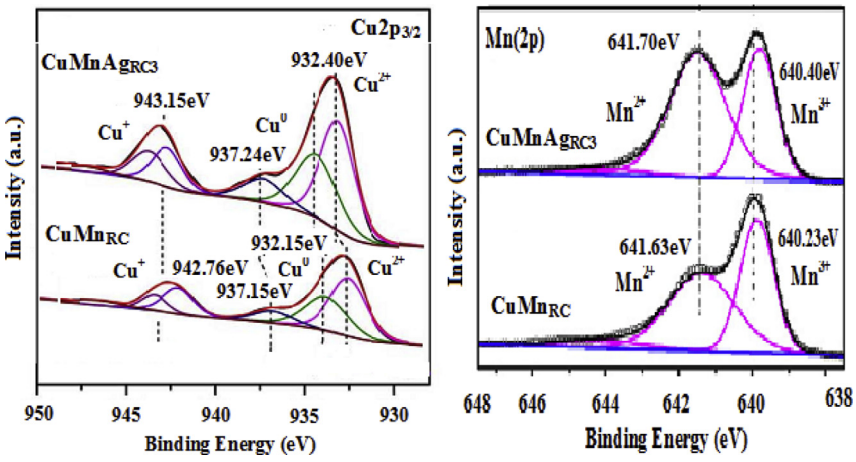


**Fig. 5.** XPS spectra of Cu(2p) and Mn (2p) in all the catalysts.

**Table 5**
Binding energy and chemical state of $CuMn_{RC}$ and $CuMnAg_{RC3}$ catalyst.

| Sample | Elements | | | |
|---|---|---|---|---|
| | Cu | Mn | O | Ag |
| $CuMn_{RC}$ | Cu(II) Oxide 932.15eV | $MnO_2$ 641.63eV | C-O 530.02eV | – |
| $CuMnAg_{RC3}$ | Cu(II) Oxide 932.40eV | $MnO_2$ 641.70eV | C-O 529.86eV | $Ag_2O$ 370.56eV |

**Table 6**
Textural property of the catalyst.

| Catalyst | Surface Area ($m^2$/g) | Pore Volume ($cm^3$/g) | Ave. Pore Size (Å) |
|---|---|---|---|
| $CuMn_{RC}$ | 127.80 | 0.640 | 73.50 |
| $CuMnAg_{RC3}$ | 145.76 | 0.676 | 60.45 |
| $CuMnAg_{FA3}$ | 121.35 | 0.583 | 78.60 |
| $CuMnAg_{SA3}$ | 108.37 | 0.438 | 86.65 |

This result was also in good agreement with EDX results. The investigation of the chemical state of Ag species present in CuMnOx catalysts was showed in Fig. 6. The binding energy of Ag $3d_{5/2}$ was 370.56 eV and $3d_{3/2}$ was 377.45 eV, which was characteristic of metallic $Ag^0$. The Cu and Mn content show a huge influence on the chemical state of Ag species. The binding energy and chemical state of $CuMn_{RC}$ and $CuMnAg_{RC3}$ catalysts were described in Table 5.

The addition of small amount of Ag into the CuMnOx catalyst increases their strength and interface between Ag species and Cu-Mn species, thus leading to the increase of binding energy. The Ag (3d) spectra in $CuMnAg_{RC3}$ catalyst has showed that two peaks at the binding energies of 370.56 eV ($Ag3d_{5/2}$) and 377.45 eV ($Ag3d_{3/2}$) were very close to the expected value of metallic Ag (370.60 and 377.48 eV), indicating that the Ag promoted on CuMnOx catalyst was mostly in the metallic state, being regular with the XRD and FTIR results. The binding energy of Ag (3d) decreases, indicating more $Ag_2O$ species were formed. The $Ag_2O$ will usually decompose into metallic Ag with the thermal treatment at the higher temperatures.

The peak area was the function of atomic numbers of an element when the XPS spectra were calculated in the similar conditions for the same Ag element. Thus, the peak area was entirely related to the number of Ag atoms in the scanning volume. When Ag was highly dispersed over the CuMnOx catalyst, there would be much Ag atoms exposed to the surface and emitted photoelectrons, consequently led to the high intensity of Ag (3d) spectral lines. The Mn (2p) and Cu(2p) core level peak positions of the $CuMnAg_{RC3}$ catalyst surface changes upon exposure to oxygen while the Ag (3d) core level position remains unchanged. The molar ratio of Ag/(Cu + Mn) in the $CuMnAg_{RC3}$ catalyst was decreased, which indicates that the Ag content decreases and more and more Ag species included into the channels. Finally, it was confirmed that the addition of small amount of Ag was valuable to the formation of small sized highly dispersed metal particles into the $CuMnAg_{RC3}$ catalyst.

### 3.6. Surface area measurement of catalyst

The surface area, pore volume and pore size of catalysts prepared in different calcination conditions highly effects on the activity of resulting catalysts. A new route of reactive calcination (127.80 $m^2$/g) was much better to those of the catalysts prepared by other calcination routes. The effect of different calcination conditions on the isotherms of CuMnAg catalyst is showed in Fig. 7. The presence of hysteresis loop atpressure ($P/P_0$) of 0.6–1.0 indicates that the porosity arising from the non-crystalline intra-aggregate voids and spaces formed by the inter-particle contacts. Fig. 7(A) indicates the surface area measurement of the catalyst and Fig. 7(B) presents the pore size distributions (PSDs) as calculated by the Barrett–Joyner–Halendar (BJH) method from the desorption branch of the nitrogen isotherms. Specific surface area and total pore volume were two major factors which can affect the catalytic activity for CO oxidation. Clearly, the textural property of the $CuMnAg_{RC3}$ catalyst was more active for CO oxidation at a low temperature. The doping of Ag into CuMnOx catalyst resulted in an improved specific surface area and total pore volume of the catalysts. The specific surface area of $CuMnAg_{SA3}$, $CuMnAg_{FA3}$ and $CuMnAg_{RC3}$ catalyst were 108.37, 121.35 and 145.76 $m^2$/g, respectively. These data clearly indicate that the Ag mainly acts as a structural promoter, which consider the high efficiency of highly dispersed Ag nanoparticles for low-temperature CO oxidation.

The pore volume and specific surface area of $CuMnAg_{RC3}$ catalyst was higher than $CuMnAg_{FA3}$ and $CuMnAg_{SA3}$ catalysts. The catalyst surface area is similar regardless of the preparation atmosphere; however, there was a general increase in surface area as a result of increasing promoter percentages.

Typically the nitrogen adsorption/desorption isotherms of these catalysts with the hysteresis loop show that the catalysts are mesopores according to De Boer classification. In mesopores, the molecules from a liquid-like adsorbed phase have a meniscus of which curvature was associated with the Kelvin equation, providing the pore size distribution calculation. The $CuMnAg_{RC3}$ catalyst surface area (145.76 $m^2$/g) and pore volume (0.676 $cm^3$/g) were highest so that it was most active for CO oxidation at low temperature. The $CuMnAg_{RC3}$ catalyst was not easily deactivated by a trace amount of moisture presented in the catalyst. A large

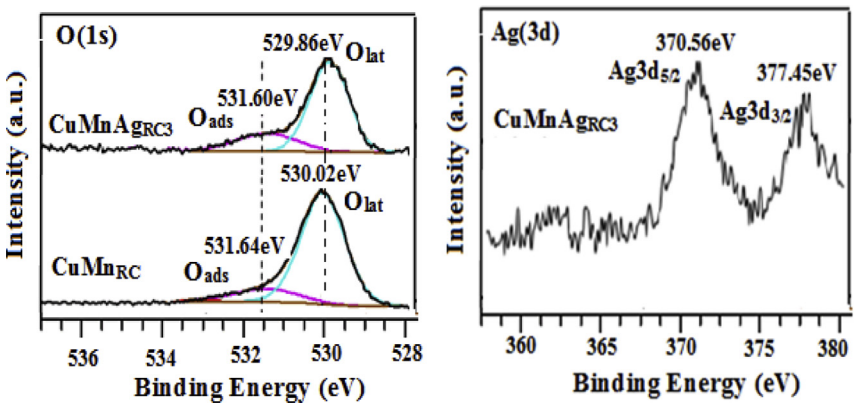


**Fig. 6.** XPS spectra of O (1s) and Ag (3d) in the catalyst.

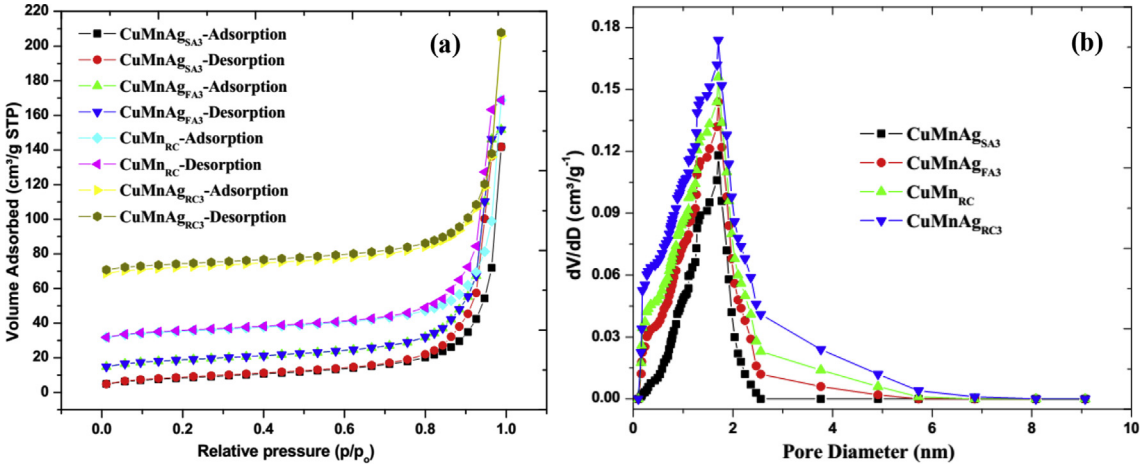


**Fig. 7.** Textural properties of (a) $N_2$ adsorption-desorption isotherms and (b) pore size distributions.

amount of pores presented on a $CuMnAg_{RC3}$ catalyst surface means a large number of CO molecules were trapped and they should show better catalytic activity at a low temperature. When the catalytic activity was measured (see later), it was found that the higher catalytic specific surface area and total pore volume resulted in the best catalytic activity. The specific surface area was measured by BET analysis was also following the SEM and XRD results.

## 4. Catalyst performance and activity measurement

Activity measurement of the catalyst was carried out to evaluate the efficiency of promoted and un-promoted CuMnOx catalysts as a function of temperature. It was measured in different calcination conditions like stagnant air, flowing air and reactive calcination. The activity was increased with the increase of temperature from room temperature to a certain high temperature for full conversion of CO. The improved catalytic activity of the catalysts can be attributed to the unique structural, textural characteristics and the smallest crystallite size.

### *4.1. Reactive calcination of the catalysts*

The recent work in our laboratory demonstrated that the two-step processes of the calcination of precursors and subsequent activation could be reduced to a single step of reactive calcination (RC) in a reactive CO-air mixture at low temperature ~160 °C. The RC process not only minimized the processing step but also produced $CuMnAg_{RC}$ catalysts with improved performance for CO oxidation. In the beginning, very slow exothermic oxidation of CO over the precursor's crystallites started causing a small rise in the local temperature, ensuing decomposition of the precursor also. The temperature was maintained for a defined period of time during which 100% CO conversion was achieved. The conversion of CO was just initiated in reactive calcination conditions at ~25 °C. Overall, the half conversion of CO (50%) using $CuMnAg_{RC3}$ catalyst was achieved at 35 °C, which was lowered by about 20 , 15 , 10 , 5 and 8 °C than that of using $CuMn_{RC}$, $CuMnAg_{RC1}$, $CuMnAg_{RC2}$, $CuMnAg_{RC4}$ and $CuMnAg_{RC5}$ catalysts, respectively. The complete conversion of CO was achieved at 55 °C using $CuMnAg_{RC3}$ catalyst, which was less by about 25 , 20 , 15 , 5 and 10 °C than that of employing $CuMn_{RC}$, $CuMnAg_{RC1}$, $CuMnAg_{RC2}$, $CuMnAg_{RC4}$ and $CuMnAg_{RC5}$ catalysts, respectively. The characterization by various techniques (XRD, SEM-EDX, XPS, FTIR and BET) of $CuMnAg_{RC}$ catalysts prepared by reactive calcination shows the presence of major $Cu_2O$, $MnO_2$ and $Ag_2O$ phases.

The exothermic initiation oxidation of CO rises the local point temperature of the catalyst to be than the measured bulk temperature. This phenomenon of oxidized adsorbed CO over the catalyst surface is lower than the bulk temperature. Thus, it was apparent from Fig. 8 that the catalysts formed by the novel route of RC of the precursors were more active for CO oxidation than the traditional method of calcination of the similar precursors in air. It was clear from Table 7 and Fig. 8 that the $CuMnAg_{RC3}$ showed the best catalytic activity for CO oxidation as compared to other catalysts. The order of activity of the catalysts for CO oxidation was as follows: $CuMnAg_{RC3}$ > $CuMnAg_{RC4}$ > $CuMnAg_{RC5}$ > $CuMnAg_{RC2}$ > $CuMnAg_{RC1}$ > $CuMn_{RC}$ (Table 8).

After the activity test, it is observed that the $CuMnAg_{RC3}$ catalyst has a higher activity for CO oxidation as compared to other catalyst samples. Finally, it was confirmed that the $CuMnAg_{RC3}$ catalyst revealed the best performance for CO oxidation at a low temperature and these systems were now worthy for further investigation.

### *4.2. Comparison of reactive calcination with traditional calcination*

A comparative study of CO oxidation over the $CuMnAg_3$ catalysts formed under various calcination conditions of stagnant air, flowing air and RC was showed in Fig. 9. It was apparent that the calcination strategies of the precursors have a drastic effect on the activity of resulting catalyst. The conversion of CO was initiated at ~25 °C, overall, the half conversion of CO using $CuMnAg_{RC3}$ catalyst

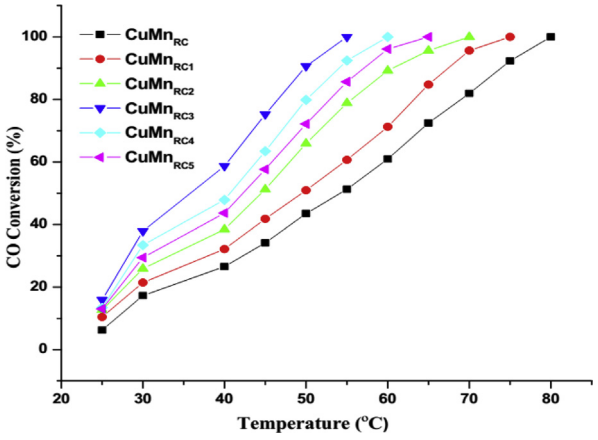


**Fig. 8.** Catalytic activities of $CuMnAg_{RC}$ catalysts for CO oxidation.

**Table 7**
Light-off characteristics of $CuMn_{RC}$ and $CuMnAg_{RC}$ catalysts.

| Catalyst | $T_i$ | $T_{50}$ | $T_{100}$ |
|---|---|---|---|
| $CuMn_{RC}$ | 25 °C | 55 °C | 80 °C |
| $CuMnAg_{RC1}$ | 25 °C | 50 °C | 75 °C |
| $CuMnAg_{RC2}$ | 25 °C | 45 °C | 70 °C |
| $CuMnAg_{RC3}$ | 25 °C | 35 °C | 55 °C |
| $CuMnAg_{RC4}$ | 25 °C | 40 °C | 60 °C |
| $CuMnAg_{RC5}$ | 25 °C | 43 °C | 65 °C |

**Table 8**
Light-off characteristics of $CuMnAg_3$ catalysts.

| Catalyst | $T_i$ | $T_{50}$ | $T_{100}$ |
|---|---|---|---|
| $CuMnAg_{SA3}$ | 25 °C | 50 °C | 100 °C |
| $CuMnAg_{FA3}$ | 25 °C | 40 °C | 90 °C |
| $CuMnAg_{RC3}$ | 25 °C | 35 °C | 55 °C |

was achieved at 35 °C, which was lowered by 15 ° and 5 °C over than that of $CuMnAg_{SA3}$ and $CuMnAg_{FA3}$ catalysts, respectively. The full conversion of CO has occurred at 55 °C for $CuMnAg_{RC3}$ catalyst, which was lowered by 35 and 45 °C over than that of $CuMnAg_{FA3}$ and $CuMnAg_{SA3}$ catalysts, subsequently. The activity order of CuMnAg catalysts for CO oxidation in the decreasing sequence was in accordance with their characterization as follows: $CuMnAg_{RC3}$ > $CuMnAg_{FA3}$ > $CuMnAg_{SA3}$. The relatively open-textured pores will be favor abble for the adsorption of reactants and desorption of products and thus facilitate the oxidation process.

The improved catalytic activity of reactive calcination can be ascribed to the unique structural and textural characteristics as the smallets crystallites of Cat-R, highly dispersed and highest specific surface area which could expose more active sites for CO oxidation.

The presence of partially reduced phase provides an oxygen deficient defective structure which can creates a high density of active sites as a result of reactive calcination and turn the $CuMnAg_{RC3}$ into the most active catalyst. Finally, we get that the RC route was the most appropriated calcination strategy for the production of highly active $CuMnAg_{RC3}$ catalyst for CO oxidation.

### 4.3. Blank experiment

A blank experiment was carried out with alpha-alumina only in place of the catalyst. At bed temperature increase up to 300 °C practically, no oxidation of CO has been observed under the experimental conditions. From the blank test, it can be confirmed that the performance of reactor in the absence of catalyst for CO oxidation and increasing of temperature does not show any activity for CO oxidation. Thus, the catalytic effect of the reactor wall and alumina used as diluents can be neglected within the experimental conditions.

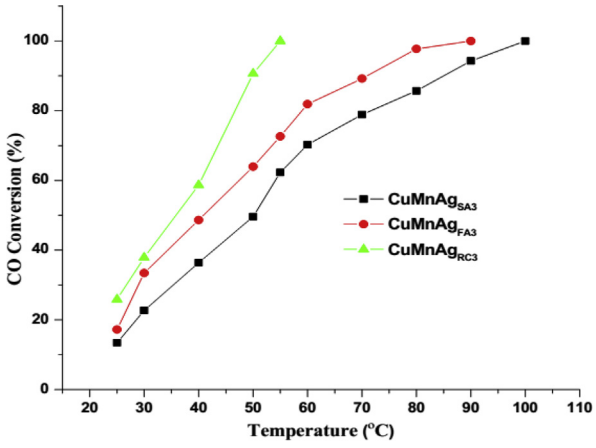


**Fig. 9.** Activity test of CuMnAg catalysts in different calcination conditions.

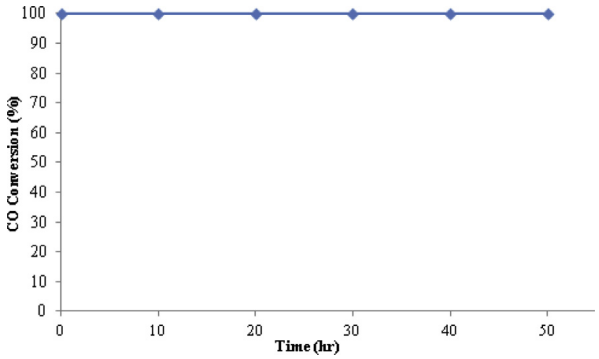


**Fig. 10.** Stability test of $CuMnAg_{RC3}$ catalyst for CO oxidation.

### 4.4. Stability test

The stability test of $CuMnAg_{RC3}$ catalyst was conducted at 55 °C for the oxidation of CO in a continuous running for 48 h under the earliest mentioned experimental conditions. The results revealed that practically no deactivation of the $CuMnAg_{RC3}$ catalyst has occurred in the experiments. In Fig. 10 we have observed that the $CuMnAg_{RC3}$ catalyst was stable for 48 h in continuous running process.

The performance of $CuMnAg_{RC3}$ catalyst was associated with the modification in intrinsic morphological, textural characteristics such as surface area, crystallite size and particle size of the catalyst. The major objective of this study was to evaluate the stability of $CuMnAg_{RC3}$ catalyst as well as their importance of $CO_2$ formation. The Ag promotion has improved the stability of CuMnOx catalyst; it creates an ideal conditions for the catalyst and even enhances the life of $CuMnAg_{RC3}$ catalyst by preventing the degradation. With an addition of Ag into the CuMnOx catalyst, no further deactivation of the catalyst has been observed. The interaction (synergetic effects) of different metal oxides dispersed on the catalyst surfaces reduces the deactivation of the catalyst. Higher activity and stability in both oxidizing and reducing atmospheres was supported on high geometric surface area substrates with minimal pressure drop.

## 5. Conclusion

The doping of Ag promoter by the deposition-precipitation method into the CuMnOx catalyst will increase the number of active sites presented on the catalyst surfaces, causing to the improved activity of the catalyst. The Ag promoted CuMnOx catalyst was tested for CO oxidation and the optimum (wt.%) percentage of Ag in CuMnOx catalyst has been found to be 3 wt.% and further increasing the doping amount of Ag can reduce the catalytic activity. The calcination strategies of the precursor have a great influence on the activity of resulting catalysts. The calcination order with respect to the performance of catalyst for CO oxidation was as follows: reactive calcination > flowing air > stagnant air. The performance of catalysts was in accordance with their characterization. The RC route was the most appropriated calcination strategy for the production of highly active $CuMnAg_{RC3}$ catalyst for CO oxidation. The improved catalyst performance at the higher doping level was found to correlate with the observed increase in surface area.

## Acknowledgments

The authors would like to express his gratitude to the Department of Civil engineering and Chemical Engineering and Technology, Indian Institute of Technology (Banaras Hindu University) Varanasi, India; for their guidance and support.

## References

[1] S. Singh, R. Prasad, Physico-chemical analysis and study of different parameters of hopcalite catalyst for CO oxidation at ambient temperature, Int. J. Sci. Eng. Res. 7 (4) (2016) 846–855.
[2] J.A. Hoskins, Carbon monoxide: the unnoticed poison of the 21st century, Indoor Built Environ. 8 (1999) 154–155.
[3] C.D. Jones, The Ambient Temperature Oxidation of Carbon Monoxide by Copper-Manganese Oxide Based Catalysts, Ph.D. Thesis, Cardiff Catalysis Institute, Cardiff University, UK, 2006.
[4] P. Singh, R. Prasad, Catalytic abatement of cold start vehicular CO emissions, Catal. Ind. 6 (2) (2014) 122–127.
[5] A.A. Mirzaei, H.R. Shaterian, M. Habibi, G.J. Hutchings, S.H. Taylor, Characterization of copper-manganese oxide catalysts: effect of precipitate ageing upon the structure and morphology of precursors and catalysts, Appl. Catal. Gen. 253 (2003) 499–508.
[6] D.V. Mahalakshmi, P. Sujatha, C.V. Naidu, V.M. Chowdary, Contribution of vehicular emissions on urban air quality: results from public strike in Hyderabad, Indian J. Radio Space Phys. 43 (2014) 340–348.
[7] A. Faiz, C.S. Weaver, M.P. Walsh, Air Pollution from Motor Vehicles, Standards and Technologies for Controlling Emissions, The World Bank Reconstruction and Development, Washington DC, 1996.
[8] M. Katz, The heterogeneous oxidation of carbon monoxide, Adv. Catal. 5 (1953) 177–216.
[9] L. Cai, Y. Guo, A. Lu, P. Branton, W. Li, The choice of precipitant and precursor in the co-precipitation synthesis of copper manganese oxide for maximizing carbon monoxide oxidation, J. Mol. Catal. Chem. 360 (2012) 35–41.
[10] B.F.F. Benjamin, P. Alphonse, Co-Mn-oxide spinel catalysts for CO and propane oxidation at mild temperature, Appl. Catal. B Environ. 180 (2016) 715–724.
[11] M. Kramer, T. Schmidt, K. Stowe, W.F. Maier, Structural and catalytic aspects of sol–gel derived copper manganese oxides as low-temperature CO oxidation catalyst, Appl. Catal. Gen. 302 (2006) 257–263.
[12] U.R. Pillai, S. Deevi, Room temperature oxidation of carbon monoxide over copper oxide catalyst, Appl. Catal. B 64 (2006) 146–151.
[13] S. Royer, D. Duprez, Catalytic oxidation of carbon monoxide over transition metal oxides, ChemCatChem 3 (2011) 24–65.
[14] T. Huang, D. Tsai, CO oxidation behavior of copper and copper oxides, Catal. Lett. 87 (2003) 173–178.
[15] J.J. Spivey, Complete catalytic oxidation of volatile organics, American Chemical SocietyAm. Chem. Soc. 26 (1987) 2165–2180.
[16] Y. Zhou, Z. Wang, C. Liu, Perspective on CO oxidation over Pd-based catalysts, Catal. Sci. Technol. 5 (2014) 69–81.
[17] N.P. Siswana, D.L. Trimm, Metal support interactions in the catalytic oxidation of carbon monoxide, Catal. Lett. 46 (1997) 27–29.
[18] R. Prasad, P. Singh, A Preview on CO oxidation over copper chromite catalysts, Catal. Rev. 54 (2) (2012) 224–279.
[19] R. Prasad, P. Singh, A novel route of single step reactive calcination of copper salts far below their decomposition temperatures for synthesis of highly active catalysts, Catal. Sci. Technol. 3 (2013) 3326–3334.
[20] A.K. Santra, D.W. Goodman, Catalytic oxidation of CO by platinum group metals: from ultrahigh vacuum to elevated pressures, Electrochim. Acta 47 (2012) 3595–3609.
[21] Y.Y. Yao, The oxidation of CO and hydrocarbons over noble metal catalysts, J. Catal. 87 (1983) 152–162.
[22] B. Solsona, G.J. Hutchings, T. Garcia, S.H. Taylor, Improvement of the catalytic performance of CuMnOx catalysts for CO oxidation by the addition of Au, New J. Chem. 28 (2004) 708–711.
[23] G.J. Hutchings, A.A. Mirzaei, R.W. Joyner, M.R.H. Siddiqui, S.H. Taylor, Ambient temperature CO oxidation using copper manganese oxide catalysts prepared by co-precipitation: effect of ageing on catalyst performance, Catal. Lett. 42 (1996) 21–24.
[24] C. Jones, K.J. Cole, S.H. Taylor, M.J. Crudace, G.J. Hutchings, Copper manganese oxide catalysts for ambient temperature carbon monoxide oxidation: effect of calcination on activity, J. Mol. Catal. Chem. 305 (2009) 121–124.
[25] Y. Tanaka, T. Utaka, R. Kikuchi, T. Takeguchi, K. Sasaki, K. Eguchi, Water gas shift reaction for the reformed fuels over Cu/MnO catalysts prepared via spinel-type oxide, J. Catal. 215 (2003) 271–278.
[26] C.T. Peng, H.K. Lia, B.J. Liaw, Y.Z. Chen, Removal of CO in excess hydrogen over $CuO/Ce_{1-X}MnxO_2$ catalysts, Chem. Eng. J. 172 (2011) 452–458.
[27] J. Lee, H. Kim, H. Lee, S. Jang, J.H. Chang, Highly efficient elimination of carbon monoxide with binary copper-manganese oxide contained ordered nanoporous silicas, Nanocale Res. Lett. 11 (2016) 2–6.
[28] S.H. Taylor, G.J. Hutchings, A.A. Mirzaei, Copper zinc oxide catalysts for ambient temperature carbon monoxide oxidation, Chem. Commun. (1999) 1373–1374.
[29] X. Zhang, K. Ma, L. Zhang, G. Yong, Y. Dai, S. Liu, Effect of precipitation method and Ce doping on the catalytic activity of copper manganese oxide catalysts for CO oxidation, Chin. J. Chem. Phys. 24 (2010) 97–102.
[30] S. Dey, G.C. Dhal, D. Mohan, R. Prasad, The effect of doping on the catalytic activity of CuMnOx catalyst for CO Oxidation, IOSR J. Environ. Sci. Toxicol. Food Technol. 10 (11) (2017) 86–94.
[31] S. Dey, G.C. Dhal, R. Prasad, D. Mohan, Total oxidation of CO by CuMnOx catalyst at a low temperature, Int. J. Sci. Eng. Res. 7 (10) (2016) 1730–1737.
[32] S. Dey, G.C. Dhal, R. Prasad, D. Mohan, Effect of nitrate metal (Ce, Cu, Mn and Co) precursors for the total oxidation of carbon monoxide, Resour. Efficient Technol. 3 (2016) 293–302.
[33] X. Zhang, Z. Qu, X. Li, M. Wen, X. Quan, D. Ma, J. Wu, Studies of silver species for low-temperature CO oxidation on $Ag/SiO_2$ catalysts, Separ. Purif. Technol. 72 (3) (2010) 395–400.
[34] S. Dey, G.C. Dhal, D. Mohan, R. Prasad, Study of Hopcalite (CuMnOx) catalysts prepared through a novel route for the oxidation of carbon monoxide at low temperature, Bull. Chem. React. Eng. Catal. 12 (3) (2017) 393–407.
[35] S. Dey, G.C. Dhal, D. Mohan, R. Prasad, Low-temperature complete oxidation of CO over various manganese oxide catalyst, Atmos. Pollut. Res. 9 (2017) 755–763.
[36] S. Dey, G.C. Dhal, D. Mohan, R. Prasad, Copper based mixed oxide catalysts (CuMnCe, CuMnCo and CuCeZr) for the oxidation of CO at low temperature, Mater. Discovery 10 (2017) 1–14.
[37] S.A. Kondrat, T.E. Davies, Z. Zu, P. Boldrin, J.K. Bartley, A.F. Carley, S.H. Taylor, M.J. Rosseinsky, G.J. Hutchings, The effect of heat treatment on phase formation of copper manganese oxide: influence on catalytic activity for ambient temperature carbon monoxide oxidation, J. Catal. 281 (2011) 279–289.
[38] S. Dey, G.C. Dhal, D. Mohan, R. Prasad, Effect of preparation conditions on the catalytic activity of CuMnOx Catalysts for CO Oxidation, Bull. Chem. React. Eng. Catal. 12 (3) (2017) 437–451.
[39] I.A. Khan, N. Sajid, A. Badshah, M.H.S. Wattoo, D.H. Anjum, CO oxidation catalyzed by Ag nanoparticles supported on $SnO/CeO_2$, J. Braz. Chem. Soc. 26 (4) (2005) 695–704.
[40] X. Cao, M. Chen, J. Ma, B. Yin, X. Xing, CO oxidation by the atomic oxygen on silver clusters: structurally dependent mechanisms generating free or chemically bonded $CO_2$, Phys. Chem. Chem. Phys. 19 (1) (2017) 196–203.
[41] Y. Qin, Z. Qu, C. Dong, N. Huang, Effect of pretreatment conditions on catalytic activity of Ag/SBA-15 catalyst for toluene oxidation, Chin. J. Catal. 38 (9) (2017) 1603–1612.
[42] S. Dey, G.C. Dhal, D. Mohan, R. Prasad, Effects of doping on the performance of CuMnOx catalyst for CO Oxidation, Bull. Chem. React. Eng. Catal. 12 (3) (2017) 370–383.
[43] D. Chen, Z. Qu, Y. Sun, K. Gao, Y. Wang, Identification of reaction intermediates and mechanism responsible for highly active HCHO oxidation on Ag/MCM-41 catalysts, Appl. Catal. B Environ. 142–143 (2013) 838–848.
[44] S. Dey, G.C. Dhal, D. Mohan, R. Prasad, R.N. Gupta, Cobalt doped CuMnOx catalysts for the preferential oxidation of carbon monoxide, Appl. Surf. Sci. 441 (2018) 303–316.
[45] H. Chen, X. Tong, Y. Li, Mesoporous Cu-Mn Hopcalite catalysts and its performance in low temperature ethylene combustion in a carbon dioxide stream, Appl. Catal. Gen. 370 (2009) 59–65.
[46] S. Dey, G.C. Dhal, D. Mohan, R. Prasad, Characterization and activity of $CuMnOx/\gamma\text{-}Al_2O_3$ catalyst for oxidation of carbon monoxide, Mater. Discovery 8 (2017) 26–34.
[47] K. Narasimharao, A. Al-Shehri, S. Al-Thabaiti, Porous $Ag\text{-}Fe_2O_3$ nanocomposite catalysts for the oxidation of carbon monoxide, Appl. Catal. Gen. 505 (2015) 431–440.
[48] Y. Hasegawa, R. Maki, M. Sano, T. Miyake, Preferential oxidation of CO on copper-containing manganese oxides, Appl. Catal. Gen. 371 (2009) 67–72.
[49] S. Dey, G.C. Dhal, D. Mohan, R. Prasad, Kinetics of catalytic oxidation of carbon monoxide over CuMnAgOx catalyst, Mater. Discovery 8 (2017) 18–25.
[50] S. Trivedi, R. Prasad, Reactive calcination route for synthesis of active $Mn–Co_3O_4$ spinel catalysts for abatement of $CO–CH_4$ emissions from CNG vehicles, J. Environ. Chem. Eng. 4 (2016) 1017–1028.
[51] G.C. Dhal, S. Dey, D. Mohan, R. Prasad, Simultaneous control of NOx-Soot by substitutions of Ag and K on perovskite ($LaMnO_3$) catalyst, Bull. Chem. React. Eng. Catal. 13 (1) (2018) 144–154.
[52] G.C. Dhal, S. Dey, D. Mohan, R. Prasad, Solution combustion synthesis of perovskite-type catalysts for diesel engine exhausts gas purification, Mater. Today Proc. 4 (2018) 10489–10493.
[53] S. Dey, G.C. Dhal, D. Mohan, R. Prasad, Effect of various metal oxides phases present in CuMnOx catalyst for selective CO oxidation, Mater. Discovery 12 (2018) 3–71.
[54] R.N. Bracewell, The Fourier Transform and its Applications, McGraw Hill, 2000.
[55] D. Baurecht, U.P. Fringeli, Quantitative modulated excitation fourier transform infrared spectroscopy, Rev. Sci. Instrum. 72 (2013) 782–3792.
[56] Y. Kauppinen, J. Partanen, Fourier Transforms in Spectroscopy, Wiley-VCH Verlag Gmbh, 2001.
[57] A. Mishra, R. Prasad, Preparation and application of perovskite catalysts for diesel soot emissions control: an overview, Catal. Rev. Sci. Eng. 56 (2014) 57–81.